Synthesis of "Solid Solution" and "Core-Shell" Type Cobalt−Platinum Magnetic Nanoparticles via Transmetalation Reactions

Jong-Il Park and Jinwoo Cheon*

Contribution from the Department of Chemistry and School of Molecular Science (BK21), Korea Advanced Institute of Science and Technology (KAIST), Taejon 305-701, Korea

Received February 6, 2001. Revised Manuscript Received May 2, 2001

Abstract: In this article, we report the synthesis of "solid solution" and "core-shell" types of well-defined Co−Pt nanoalloys smaller than 10 nm. The formation of these alloys is driven by redox transmetalation reactions between the reagents without the need for any additional reductants. Also the reaction proceeds selectively as long as the redox potential between the two metals is favorable. The reaction between $Co_2(CO)_8$ and $Pt(hfac)_2$ (hfac = hexafluoroacetylacetonate) results in the formation of "solid solution" type alloys such as $CoPt_3$ nanoparticles. On the other hand, the reaction of Co nanoparticles with $Pt(hfac)_2$ in solution results in "Co_{core}-Pt_{shell}" type nanoalloys. Nanoparticles synthesized by both reactions are moderately monodispersed ($\sigma < 10\%$) without any further size selection processes. The composition of the alloys can also be tuned by adjusting the ratio of reactants. The magnetic and structural properties of the obtained nanoparticles and reaction byproducts are characterized by TEM, SQUID, UV/vis, IR, EDAX, and XRD.

Introduction

Nanoparticle-based materials have drawn interest due to the novel optoelectronic, magnetic, and catalytic properties that arise from the quantum size effects and large surface areas that are characteristic of these species.[1] In particular, recent efforts have been focused on the development of magnetic nanoalloys due to the potential use of each nanoparticle as an independent magnetic bit for future information storage systems.[2−5] The magnetic and chemical properties of the monometallic elements are known to be significantly enhanced by the formation of alloys with additional metals and they provide many advantages such as high magnetic anisotropy, enhanced magnetic susceptibility, and large coercivities.[4−7] Specifically, the CoPt alloy is one of the candidates for ultrahigh-density magnetic recording media because of its high magnetic anisotropy and good chemical stability upon corrosion.[4,6,7]

Most of the magnetic alloy syntheses to date have been focused in the area of thin films by using vacuum deposition techniques.[7] However, random nanoparticle nucleation and growth, relatively large crystalline sizes, and broad size distributions adversely affect their magnetic performances. Recent reports suggest chemical approaches in solution as excellent alternative methods for better control of magnetic nanomaterials growth.[5,6] For example, solid solution type MPt (M = Co or Fe) nanoparticle alloys have been successfully synthesized by adding ionic salt type or organometallic precursors to reductants such as borohydride, or diols.[4,5]

One unique way of synthesizing alloy materials on the micron scale is the redox transmetalation process as reported for the thin films of Pd, Rh, Pt/Cu,[8] and Cu/Co.[9] However, the application of this concept to nanoscale materials is unprecedented.

In this report, we demonstrate the first utilization of redox transmetalation reactions for the synthesis of two different types, solid solution and core-shell, of CoPt nanoalloys under 10 nm (Scheme 1). Stoichiometry tuned solid solution type CoPt nanoalloys are synthesized by the reaction between $Co_2(CO)_8$ and $Pt(hfac)_2$. Core-shell type nanoalloys in which Pt resides as a shell around a cobalt nanoparticle core are achieved by the reaction of $Pt(hfac)_2$ with cobalt nanoparticles. The obtained nanoalloys are moderately monodispersed (<10%) without any further size selection processes.

Experimental Section

General Methods. All procedures were carried out using standard airless techniques under argon. $Pt(hfac)_2$ and dodecane isocyanide were

(1) (a) Schmid, G. In *Clusters and Colloids. From Theory to Applications*; VCH: Wienheim, 1994. (b) Leslie-Pelecky, D. L.; Rieke, R. D. *Chem. Mater.* **1996**, *8*, 1770. (c) Alivisatos, A. P. *J. Phys. Chem.* **1996**, *100*, 13226. (d) Alivisatos, A. P. *Science* **1996**, *271*, 933.

(2) (a) Jacoby, M. *C&E News* **2000**, *78*, 37. (b) Wood, R. *IEEE Trans. Magn.* **2000**, *36*, 36.

(3) (a) Sun, S.; Murray, C. B. *J. Appl. Phys.* **1999**, *85*, 4325. (b) Pileni, M. P. *Phys. Rev. B* **2000**, *62*, 3910. (c) Papiper, E.; Horny, P.; Balard, H.; Anthore, R.; Petipas, C.; Martinet, A. *J. Colloid Interface Sci.* **1983**, *94*, 207.

(4) (a) Ely, T. O.; Pan, C.; Amiens, C.; Chaudret, B.; Dassenoy, F.; Lecante, P.; Casanove, M.-J.; Mosset, A.; Respaud, M.; Broto, J.-M. *J. Phys. Chem. B* **2000**, *104*, 695. (b) Carpenter, E. E.; Seip, C. T.; O'Connor, C. J. *J. Appl. Phys.* **1999**, *85*, 5184.

(5) (a) Carpenter, E. E.; Sims, J. A.; Wienmann, J. A.; Zhou, W. L.; O'Connor, C. J. *J. Appl. Phys.* **2000**, *87*, 5615. (b) Sun, S.; Murray, C. B.; Weller, D.; Folks, L.; Moser, A. *Science* **2000**, *287*, 1989.

(6) Liou, S. H.; Huang, S.; Klimek, E.; Kirby, R. D.; Yao, Y. D. *J. Appl. Phys.* **1999**, *85*, 4334.

(7) (a) Thielen, M.; Kirsch, S.; Weinforth, A.; Carl, A.; Wassermann, E. F. *IEEE Trans. Magn.* **1998**, *34*, 1009. (b) Yamada, Y.; Suzuki, T.; Abarra, E. N. *IEEE Trans. Magn.* **1998**, *34*, 343.

(8) (a) Lin, W.; Benjamin, C. W.; Nuzzo, R. G.; Girolami, G. S. *J. Am. Chem. Soc.* **1993**, *115*, 11634. (b) Lin, W.; Benjamin, C. W.; Nuzzo, R. G.; Girolami, G. S. *J. Am. Chem. Soc.* **1996**, *118*, 5977. (c) Lin, W.; Benjamin, C. W.; Nuzzo, R. G.; Girolami, G. S. *J. Am. Chem. Soc.* **1996**, *118*, 5988. (d) Crane, E. L.; You, Y.; Nuzzo, R. G.; Girolami, G. S. *J. Am. Chem. Soc.* **2000**, *122*, 3422.

(9) (a) Cu, S.; Yao, X.; Hampden-Smith, M. J.; Kodas, T. T. *Chem. Mater.* **1998**, *10*, 2145. (b) Gu, S.; Atanasova, P.; Hampden-Smith, M. J.; Kodas, T. T. *Thin Solid Films* **1999**, *340*, 45.

10.1021/ja0156340 CCC: $20.00
Published on Web 05/25/2001

Scheme 1. Synthetic Routes of Core-Shell and Solid Solution Type Nanoalloys via Transmetalation Reaction

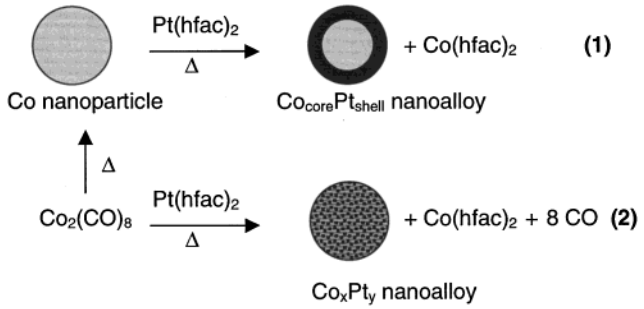

prepared according to literature methods.[10] Toluene and nonane were purified by distillation under an argon atmosphere over sodium. Ethanol was purified by distillation over calcium hydride. Solvents were carefully degassed by the freeze−pump−thaw technique before use. All other reagents purchased from commercial sources were used as obtained without further purification.

Synthesis of Nanoalloys. (a) Co_1Pt_3 Nanoalloys.[11] 0.25 mmol (0.085 g) of $Co_2(CO)_8$ (0.25 mmol, 0.085 g) in 5 mL of toluene was injected into 5 mL of hot toluene solution containing 0.5 mmol (0.28 g) of $Pt(hfac)_2$ with 0.15 mL of oleic acid as a stabilizing surfactant. Upon mixing, evolution of CO gas and a gradual color change from yellow to brownish black were observed. After 12 h, the resulting solution was cooled to room temperature and treated with ethanol to isolate the black nanocrystals from the orange supernatant. The reaction byproducts were separated from the remaining orange supernatant solution and further purified by sublimation under vacuum. The orange crystals obtained were analyzed by spectroscopic methods and elemental analysis. IR spectra of the orange crystals revealed peaks at 1645 (C═O str), 1610 (C═C str), 1564 (C═O str, C═C bend), 1537 (C═O str, C═C bend), 1485 (C═O str, C═C bend), 1347 (CF_3 str), 1258 (CF_3 str), 1227 (CF_3 str), 1205 (C−H in plane bend), 1146 (C−H in plane bend), 1095 (C−H out of bend), 805 (C−H out of bend), 744 (C−CF_3 str), and 674 (C−CF_3 str) cm^{-1}. UV/vis absorption maxima occurred at 300 nm from a $\pi-\pi^*$ transition and at 455(sh), 489, 510, and 546 nm from d−d transitions. Elemental Anal. Calcd for $C_{10}H_2O_4F_{12}Co\cdot xH_2O$ ($x = 1.5$): C, 24.02; H, 1.01; Co, 11.79. Found: C, 24.16; H, 1.24; Co, 11.58. The obtained Co_1Pt_3 nanoparticles are easily redispersed in organic solvent such as hexane and toluene.

(b) Co_1Pt_1 Nanoalloys. The Co_1Pt_1 alloy was synthesized using the same procedure used to synthesize Co_1Pt_3 nanoalloys except with modified reagent ratios. Co_1Pt_1 is obtained from 0.5 mmol (0.170 g) of $Co_2(CO)_8$ and 0.5 mmol (0.28 g) of $Pt(hfac)_2$.

(c) $Co_{core}Pt_{shell}$ Nanoalloys. $Co_{core}Pt_{shell}$ nanoalloys were synthesized by refluxing 6.33 nm ($\sigma = 0.61$) Co nanoparticle colloids (0.5 mmol) and $Pt(hfac)_2$ (0.25 mmol) in a nonane solution containing 0.06 mL of $C_{12}H_{25}NC$ as a stabilizer. The Co nanoparticles were synthesized from the thermolysis of $Co_2(CO)_8$ in toluene solution.[12] After 8 h of reflux, the colloids are isolated from the dark red-black solution in powder form after adding ethanol and centrifugation. Reaction byproduct was separated and analyzed as $Co(hfac)_2$. The nanoparticles obtained are stable in air and can be redispersed in typical organic solvents.

Characterization. Transmission electron microscopy (TEM) observations were carried out on an EM 912 Omega and Hitachi H9000-NAR high-resolution electron microscope operated at 120 or 300 kV, respectively. Elemental analysis was performed on an inductively coupled plasma atomic emission spectrometer (Shimadzu ICPS-1000III) and elemental analyzer (EA1110-FISONS). Infrared spectra were obtained by an EQUINOX 55 FT-IR spectrometer (KBr pallet). UV/vis absorption data were obtained by a Shimadzu UV-3100S spectrophotometer in EtOH solvent. Powder X-ray diffraction (XRD) spectra were obtained using graphite-monochromatized Cu Kα radiation in a Rigaku D/MAX-RC diffractometer operated at 40 kV 80 mA. Magnetic measurements were performed on a SQUID magnetometer (Quantum Design MPMS-7). DC susceptibility and hysteresis measurements were recorded for powdered samples of nanoparticles in a gelatin capsule. The temperature was varied between 5 and 300 K according to a zero field cooling/field cooling (ZFC/FC) procedure at 75 Oe, and the hysteretic loops were obtained in a magnetic field varying from +5 to −5 T.

Results and Discussion

The size distribution and crystallinity of the nanoparticles were studied first by transmission electron microscopy. TEM images show the presence of nonagglomerated and moderately monodispersed spherically shaped $CoPt_3$ nanoparticles with an average diameter of 1.8 nm ($\sigma = 0.1$ nm) (Figure 1). Examination of single nanoparticles (Figure 1 inset) gives lattice spacings of 2.23(±0.03) Å for the (111) plane and 1.93(±0.03) Å for the (200) plane, which are consistent with the known bulk fcc values.[13] X-ray powder diffraction and selected area electron diffraction (SAED) patterns also show peaks due to the (111), (200), (220), and (311) lattice planes of fcc $CoPt_3$. Elemental analysis of the nanoparticles confirms that the ratio of Co to Pt is 1.00:2.96. Similar results were obtained for Co_1Pt_1 with homogeneous nanoparticles (1.9 nm, $\sigma = 0.3$ nm) by TEM analyses and a Co-to-Pt ratio of 0.46:0.54 is obtained from energy-dispersive X-ray analysis (EDAX), which is close to the expected 1:1 stoichiometry.

In the case of $Co_{core}Pt_{shell}$ type nanoalloys, moderately monodispersed nanoparticles with an average diameter of 6.27 nm ($\sigma = 0.58$ nm) are observed by TEM (Figure 2). The surface of the $Co_{core}Pt_{shell}$ particle is smooth and homogeneous as examined by HRTEM. This is in contrast to previous attempts which resulted in rather inhomogeneous surfaces with uneven adhesions of smaller outer particles as shell layers of core-shell nanoparticles.[14] The measured lattice distance of 2.27(±0.03) Å on the shell of nanoparticles is consistent with the known Pt lattice parameter (2.265 Å) for the (111) plane (Figure 2). While the size of the $Co_{core}Pt_{shell}$ nanoparticles remains similar to that of the starting Co nanoparticles, EDAX studies indicate that large amounts of Pt are present in the $Co_{core}Pt_{shell}$ nanoparticles with an observed stoichiometry of $Co_{0.45}Pt_{0.55}$. With this stoichiometry, the Co core is estimated to be roughly 4.75 nm with the outer Pt layer to be about 1.82 nm thick (∼4 layers) by simple close packing model simulations. In principle, the thickness of the Pt shell can be tuned by varying the amount of $Pt(hfac)_2$.

Magnetic measurements of the nanoalloys were performed on a SQUID magnetometer. A blocking temperature (T_B) of 20 K (Figure 3) and a coercivity (H_c) of 6900 Oe at 5 K (Figure 4) were observed for $CoPt_3$ nanoalloys while a T_B of 15 K and H_c of 5300 Oe at 5 K (Figure 4) were observed for Co_1Pt_1 nanoalloys. These values are higher relative to those observed for pure cobalt nanoparticles of similar size[12a,15] as a result of the increased anisotropy due to alloy formation. These solid solution type nanoparticles show superparamagnetic behavior at 300 K.

(10) (a) Okeya, S.; Kawaguchi, S. *Inorg. Synth.* **1980**, *20*, 65. (b) Weber, W. P.; Gokel, G. W. *Tetrahedron Lett.* **1972**, *13*, 1637.

(11) Our synthetic method appears at a glimpse similar to the FePt synthesis by Sun et al. (ref 5b), but the two methods in fact employ different processes. Our process utilizes a redox transmetalation process between $Pt(hfac)_2$ and Co metals for Pt generation, whereas their work is based on the "polyol process" in the $Pt(acac)_2$ reduction step.

(12) Park, J.-I.; Cheon, J. Unpublished results. (a) $T_B = 10$ K and $H_c = 260$ Oe for 2.2 nm Co; (b) $T_B = 100$ K and $H_c = 470$ Oe for 6.4 nm Co; (c) $T_B = 20$ K and $H_c = 370$ Oe for 4.0 nm Co nanoparticles, respectively.

(13) X-ray Powder Diffraction Patterns (International Centre for Diffraction Data, Newtown Square, PA, 1996).

(14) (a) Schmid, G.; Lehnert, A.; Malm, J.-O.; Bovin, J.-O. *Angew. Chem., Int. Ed. Engl.* **1991**, *30*, 874. (b) Schmid, G.; West, H.; Mehles, H.; Lehnert, A. *Inorg. Chem.* **1997**, *36*, 891. (c) Wang, Y.; Toshima, N. *J. Phys. Chem. B* **1997**, *101*, 5301.

(15) When compared to other known values of $CoPt_3$, our H_c value is comparable within the same order of magnitude.

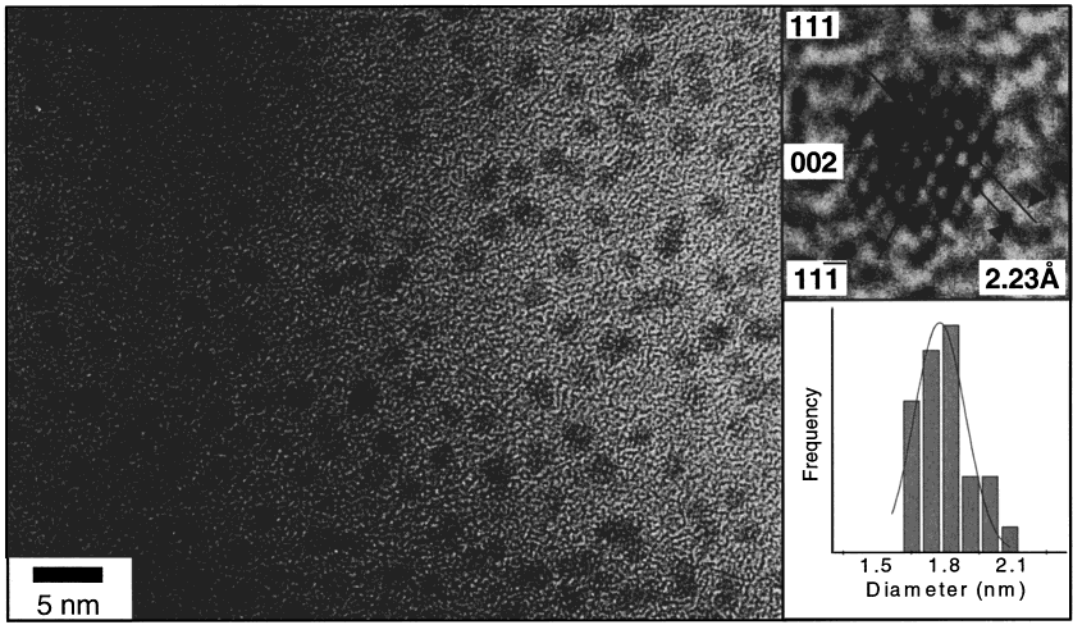

Figure 1. High-resolution TEM images and histogram of 1.8 nm ($\sigma = 0.1$) $CoPt_3$ nanoalloys.

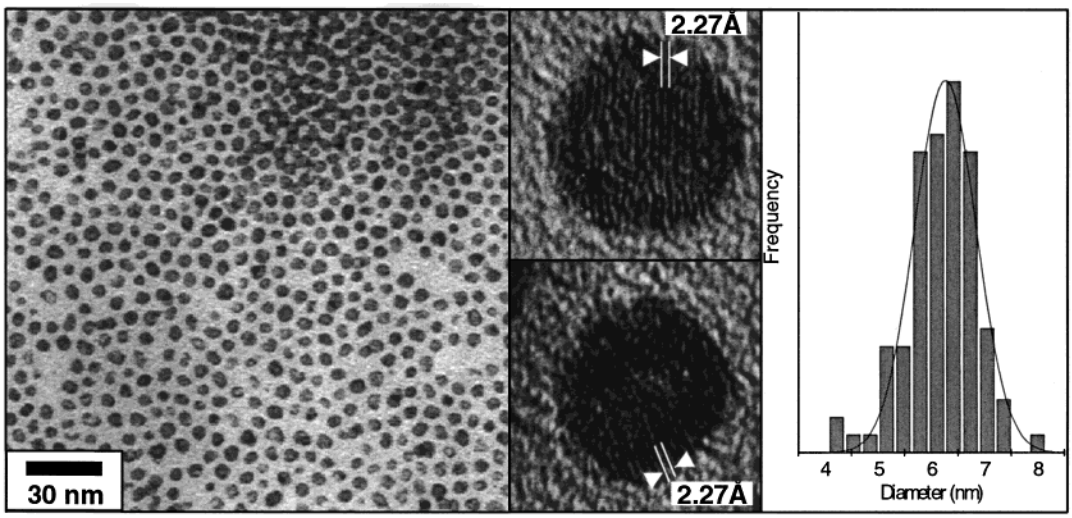

Figure 2. TEM, HRTEM images, and histogram of 6.27 nm ($\sigma = 0.58$) $Co_{core}Pt_{shell}$ nanoalloys.

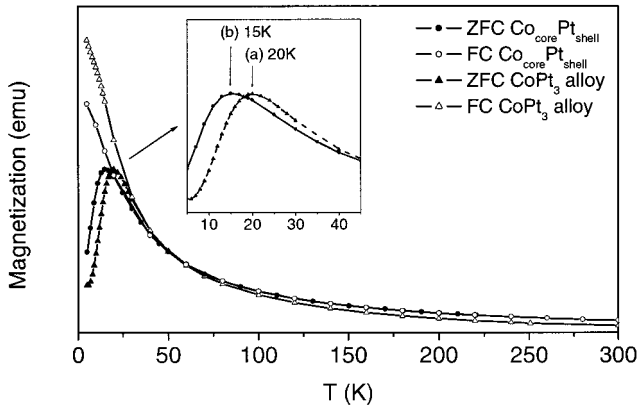

Figure 3. ZFC/FC curves of (a) $Co_{core}Pt_{shell}$ and (b) $CoPt_3$ nanoalloys. $T_B = 15$ K for the $Co_{core}Pt_{shell}$ and $T_B = 20$ K for the $CoPt_3$ are observed.

Magnetic studies performed on the $Co_{core}Pt_{shell}$ nanoalloys indicate that these structures retain the properties of the pure Co core and are not significantly affected by the Pt shell. A T_B value of 15 K (Figure 3) and a coercivity of 330 Oe at 5 K (Figure 4) for the $Co_{core}Pt_{shell}$ nanoalloys are smaller than those observed for similar sized Co nanoparticles,[12b] but are rather close to values for Co nanoparticles similar in size to the Co_{core}.[12c] Magnetic properties are known to be very sensitive to parameters such as the size, surface states, and compositions and we are currently investigating the factors governing magnetism in our Co−Pt nanoalloys.

The major reaction byproduct obtained from the reaction mixture during both the solid solution and core-shell of CoPt alloy preparations was analyzed and confirmed as $Co(hfac)_2$. UV/vis absorption bands (Figure 5a) due to $\pi \rightarrow \pi^*$ transition of the hfac ligand and the d → d transitions of cobalt metal complexes are observed from the isolated orange byproduct and the IR modes (Figure 5b) are cleanly matched with those of $Co(hfac)_2$.[16] Elemental analysis of the byproduct is also consistent with the $Co(hfac)_2$. Any peaks due to the reactant $Pt(hfac)_2$ are not observed. This result clearly shows that reactant $Pt(hfac)_2$ has been completely consumed and $Co(hfac)_2$ is now obtained after the reaction.

(16) (a) Morris, M. L.; Moshier, R. W.; Sievers, R. E. *Inorg. Chem.* **1963**, *2*, 411. (b) Cotton, F. A.; Holm, R. H. *J. Am, Chem. Soc.* **1960**, *82*, 2979.

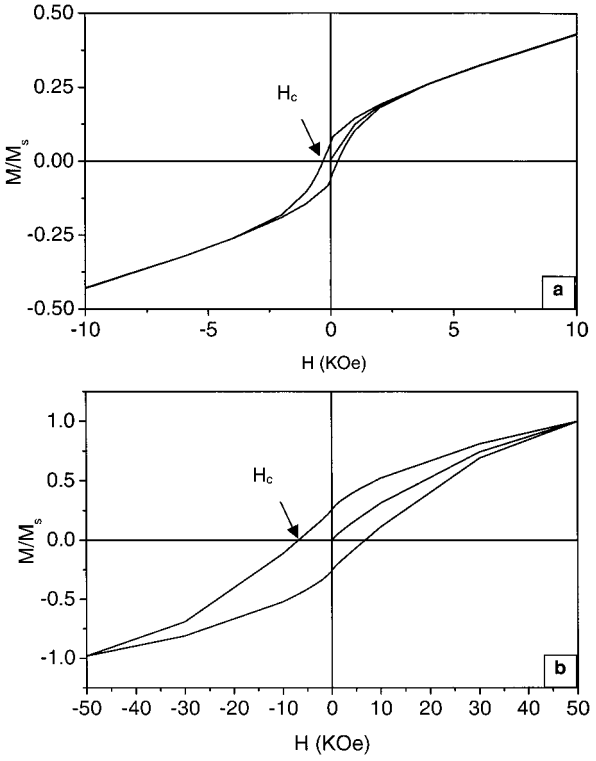

Figure 4. Hysteresis loops of (a) $Co_{core}Pt_{shell}$ and (b) $CoPt_3$ nanoalloys at $T = 5$ K. $H_c = 330$ Oe for $Co_{core}Pt_{shell}$ and $H_c = 6900$ Oe for $CoPt_3$ are observed.

Our experimental results suggest that the formation of CoPt alloys proceeds according to the redox transmetalation reaction between Co and $Pt(hfac)_2$ without the need of additional reducing reagents.[11] As a Pt layer grows around the Co core, a stoichiometric fraction of Co metal is replaced by Pt through a transmetalation process in which the hfac ligands of $Pt(hfac)_2$ are transferred to Co metal to form $Co(hfac)_2$ (Scheme 1).[17] This is in part supported by the fact that the calculated standard potential of +1.46 V for the cell $Co/Co^{2+}//Pt^{2+}/Pt$ thermodynamically favors the formation of CoPt(0) and $Co(II)(hfac)_2$.[18] A similar process is also operative in the CoPt solid solution alloy formation following metallic Co formation from $Co_2(CO)_8$ decomposition.[3c] The resulting Co atoms (or seed clusters) would undergo transmetalation reactions with $Pt(hfac)_2$ to form solid solution type alloys. In comparison, we have tried similar reactions with 7 nm Au nanoparticles with $Pt(hfac)_2$, but did not observe any kind of Au/Pt alloy formation possibly due to unfavorable redox potentials.[19] We are currently investigating the full mechanistic studies for the formation of nanoalloys by spectroscopic techniques such as EXAFS.

(17) Similar ligand transfer between metals has been reported previously. (ref 8)

(18) Vanýsek, P. In *Handbook of Chemistry and Physics*, 76th ed.; CRC Press; Boca Raton, FL, 1995; pp 8−21.

(19) Reduction potential for the cell $Au/Au^{+}//Pt^{2+}/Pt$ or $Au/Au^{3+}//$ is −0.512 or −0.318 V, respectively, from ref 18.

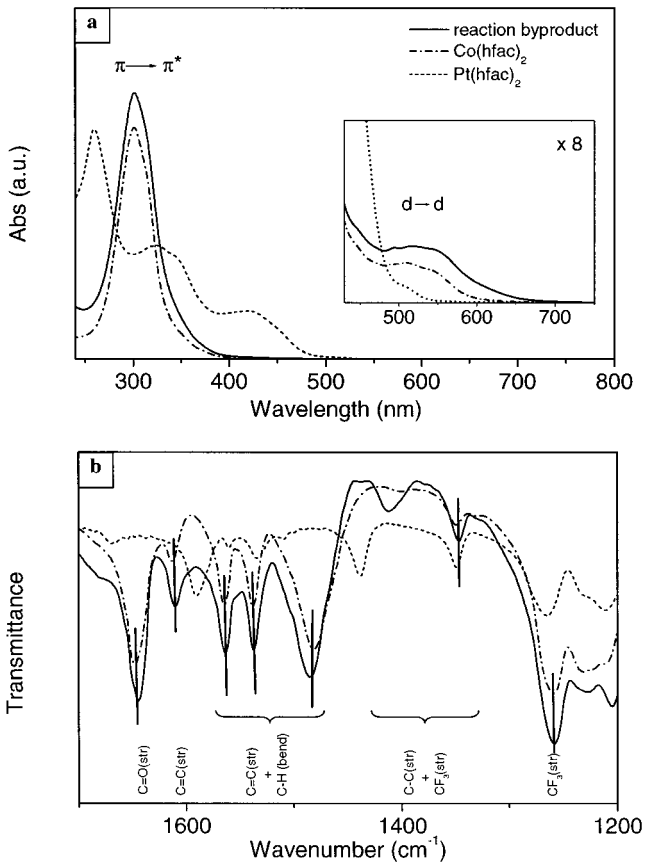

Figure 5. (a) UV/Vis absorption and (b) IR spectra of the reaction byproduct (−), $Co(hfac)_2$ (-·-), and $Pt(hfac)_2$ (···).

In summary, we report the first synthesis of both solid solution and core-shell types of magnetic nanoparticle alloys via transmetalation reactions. It is possible to selectively grow certain metals on top of metallic nanoparticles only where the redox potential is favorable between them. This kind of redox transmetalation strategy can be adapted as a general method to synthesize various types of nanoalloys with controlled composition in a selective fashion. In particular, since these magnetic alloys are monodispersed with a particle size of less than 10 nm scales, it is possible to have them in multidimensional arrays for magnetoelectronic nanodevice applications that can fulfill the next generation requirements.

Acknowledgment. This work was supported by Korea Research Foundation Grant KRF-2000-015-DS0023. We thank KBSI for the TEM and magnetic measurements of the samples. We also thank Mr. Daniel Byun for his helpful discussions.

Supporting Information Available: TEM images of Co_1-Pt_1 and Co nanoparticles and EDAX analysis (PDF). This material is available free of charge via the Internet at http://pubs.acs.org.

JA0156340